Journal of
Sensor and Actuator Networks

MDPI

Article

Characteristic-Mode-Analysis-Based Compact Vase-Shaped Two-Element UWB MIMO Antenna Using a Unique DGS for Wireless Communication

Subhash Bodaguru Kempanna [1], Rajashekhar C. Biradar [1], Praveen Kumar [2], Pradeep Kumar [3], Sameena Pathan [4] and Tanweer Ali [2,*]

[1] School of ECE, REVA University, Bangalore 560064, India
[2] Department of Electronics and Communication Engineering, Manipal Institute of Technology, Manipal Academy of Higher Education, Manipal 576104, India
[3] Discipline of Electrical, Electronic and Computer Engineering, University of KwaZulu-Natal, Durban 4041, South Africa; kumarp@ukzn.ac.za
[4] Department of Information and Communication Technology, Manipal Institute of Technology, Manipal Academy of Higher Education, Manipal 576104, India
* Correspondence: tanweer.ali@manipal.edu

Abstract: The modern electronic device antenna poses challenges regarding broader bandwidth and isolation due to its multiple features and seamless user experience. A compact vase-shaped two-port ultrawideband (UWB) antenna is presented in this work. A circular monopole antenna is modified by embedding the multiple curved segments onto the radiator and rectangular slotted ground plane to develop impedance matching in the broader bandwidth from 4 to 12.1 GHz. The UWB monopole antenna is recreated horizontally with a separation of less than a quarter wavelength of 0.13 λ (λ computed at 4 GHz) to create a UWB multiple input and multiple output (MIMO) antenna with a geometry of $20 \times 29 \times 1.6$ mm^3. The isolation in the UWB MIMO antenna is enhanced by inserting an inverted pendulum-shaped parasitic element on the ground plane. This modified ground plane acts as a decoupling structure and provides isolation below 21 dB across the 5–13.5 GHz operating frequency. The proposed UWB MIMO antenna's significant modes and their contribution to antenna radiation are analyzed by characteristic mode analysis. Further, the proposed antenna is investigated for MIMO diversity features, and its values are found to be ECC < 0.002, DG ≈ 10 dB, TARC < -10 dB, CCL < 0.3 bps/Hz, and MEG < -3 dB. The proposed antenna's time domain characteristics in different antenna orientations show a group delay of less than 1 ns and a fidelity factor larger than 0.9.

Keywords: ultrawideband (UWB); MIMO; isolation; CMA; DGS

check for updates

Citation: Kempanna, S.B.; Biradar, R.C.; Kumar, P.; Kumar, P.; Pathan, S.; Ali, T. Characteristic-Mode-Analysis-Based Compact Vase-Shaped Two-Element UWB MIMO Antenna Using a Unique DGS for Wireless Communication. *J. Sens. Actuator Netw.* **2023**, *12*, 47. https://doi.org/10.3390/jsan12030047

Academic Editors: Teen-Hang Meen, Charles Tijus, Cheng-Chien Kuo, Kuei-Shu Hsu, Kuo-Kuang Fan and Jih-Fu Tu

Received: 22 May 2023
Revised: 13 June 2023
Accepted: 14 June 2023
Published: 15 June 2023

1. Introduction

The advancement of technology intensely depends on wireless communication. The existing narrow bands, such as Bluetooth and WiFi, are overcrowded, and almost all electronic gadgets utilize these frequency bands. The allocation of unregulated ultrawideband (UWB) frequency from 3.1 to 10.6 GHz for commercial purposes has attracted antenna researchers and those from cellular, automotive, and medical industry sectors. The UWB communication system has merits, such as a high data rate, low power consumption, and ability to penetrate obstacles over the existing narrow bands [1]. The antenna researcher widely accepts monopole-printed antennas for developing UWB antennas. However, these antennas inherently provide narrow bandwidth [2]. To develop a wider impedance bandwidth from 3.1 to 10.6 GHz, the antenna's ground plane is lowered. The modification of the ground plane affects the uniform current distribution, resulting in a decreased quality factor and increased bandwidth. The enhanced bandwidth achieved by lowering the ground plane applies to only higher frequency ranges. Achieving bandwidth towards a lower frequency is challenging in terms of compactness. The multiple curved boundary segments incorporated into the patch help to develop bandwidth at a lower frequency. The perimeter of the radiator is inversely proportional to the lower frequency. Therefore, increasing the radiator's perimeter shifts the operating frequency towards the lower side. The literature illustrates various antenna structures operating in the UWB spectrum. The fractal radiator and defected ground structure (DGS) are utilized to extend the impedance bandwidth from 3.77 to 11.4 GHz [3]. The antenna's ground plane is tapered, lowered, and a rectangular slot is created to develop broader bandwidth. A modified square radiator fed by a microstrip line with the lowered ground plane UWB antenna is demonstrated in [4]. The ground plane is defected by a slot to extend the operating frequency from 1.8 to 15.2 GHz. The antenna operating between frequencies of 3 and 10 GHz is shown in [5]. The rectangular patch is modified with the lowered ground plane to help aid the UWB spectrum. A glass monopole antenna operating in the UWB is discussed in [6]. The antenna has a lowered ground plane with a U-shaped slot to operate in the frequency range of 1.17–4.49 GHz. A rectangular patch coplanar waveguide-fed antenna was modified to a paddle-shaped radiator, as demonstrated in [7]. The parasitic elements and the metamaterial unit cell are used for developing wider impedance bandwidth and enhancing gain.

The UWB system uses short pulses (ns) for communication. It may lead to, first, the multipath fading and, second, frequency domain analysis not being enough to describe the efficacy of the UWB antenna. Therefore, the time domain features that describe the output signal's phase linearity, transfer function, and faithful reproduction must be evaluated. Multiple input and multiple output (MIMO) technologies are widely used in UWB communication systems to improve the system's capacity, increase data rate, and enhance the reliability of wireless communication. The performance of the UWB MIMO system depends on the design and performance of the MIMO antenna. The proximity placement of the antenna inherently provides mutual coupling. Therefore, designing an efficient and effective UWB MIMO antenna is crucial for the UWB communication system. Various approaches, such as defected ground structure (DGS), decoupling network, neutralization line (NL), filters, metamaterial loading, or a combination of two or more of the methodologies mentioned above, were demonstrated in earlier work to improve the isolation. The rectangular patch is defected using the circle at the lower end with CPW to realize the UWB frequency of the operation in [8]. The designed UWB antenna is converted to a four-port MIMO by placing antennas in an orthogonal orientation. The isolation among the ports is increased by embedding a parasitic element, resulting in isolation better than 21 dB. Modified hexagonal UWB antennas with DGS are arranged orthogonally to form a four-port UWB antenna [9]. The orthogonal configuration of the antenna design provides isolation better than 15 dB across operating frequencies of 2.84–15.88 GHz. A modified circular patch with DGS, as demonstrated in [10], offers an impedance bandwidth of 3–20 GHz with an isolation of 23 dB. Enhanced isolation is achieved by modifying the ground plane and parasitic elements between the antennas. The antenna's ground plane, presented in [11], has a slot on the ground plane to improve the isolation of 20 dB. The antennas mentioned above have either larger geometry or orthogonal placement without a connected ground as the demerits [12]. The UWB MIMO antenna, using parasitic elements and DGS to reduce the mutual coupling, is demonstrated in [13–15].

This work presents a compact two-port UWB antenna with a geometry of $20 \times 29 \times 1.6$ mm^3 with the modified ground plane for isolation enhancement. The conventional circular monopole antenna is modified by incorporating rectangles and circles with a slotted lowered ground plane to attain frequencies of operation of 4–12.4 GHz. The UWB antenna is recreated horizontally with a separation of 0.16 λ (λ computed at 4 GHz) to create a UWB MIMO antenna. The proposed two-port antenna operates from 5 to 13.5 GHz with an average isolation better than 21 dB. The remainder of this paper is organized as follows: The antenna design methodology is described in Section 2. The optimal values of the antenna are selected by performing the comprehensive parametric analysis and are discussed in Section 3. Section 4 illustrates the characteristic mode analysis of the proposed antenna. The computational and experimental findings are presented in Section 5. Section 6 interprets the comparative analysis of the proposed antenna with the previous work. The concluding remarks are presented in Section 7.

2. Antenna Design

The conventional circular monopole antenna with a radius of 5.6 mm with a full ground plane is initially designed and simulated. To realize the broader frequency of operation, a circular patch is modified by embedding the ellipse between the feedline and patch onto the radiator. Further, the radiator is carved using circles on the left, right, and top, with the ground plane, lowered sequentially in association with the reflection coefficient (S11) curve. Further, a U-shaped slot is carved from the ground plane to achieve a wider impedance bandwidth. The evolutional stages of the radiator and its S11 curves are depicted in Figure 1. The antenna in iteration A1 has an operational frequency of 3.2–6 GHz and is due to the modification of the ground plane. In the second iteration A2, an ellipse is embedded between the feedline and radiator. This configuration provides wider bandwidth, but at the center frequency, the S11 curve falls short of lying below the −10 dB line. Further, the radiator is truncated on the left and right side by the arcs as in iteration A3 of Figure 1a. In a similar manner, an arc etches the proposed antenna radiator's upper part, and this arrangement provides wider bandwidth below −12 dB from 4–12.1 GHz.

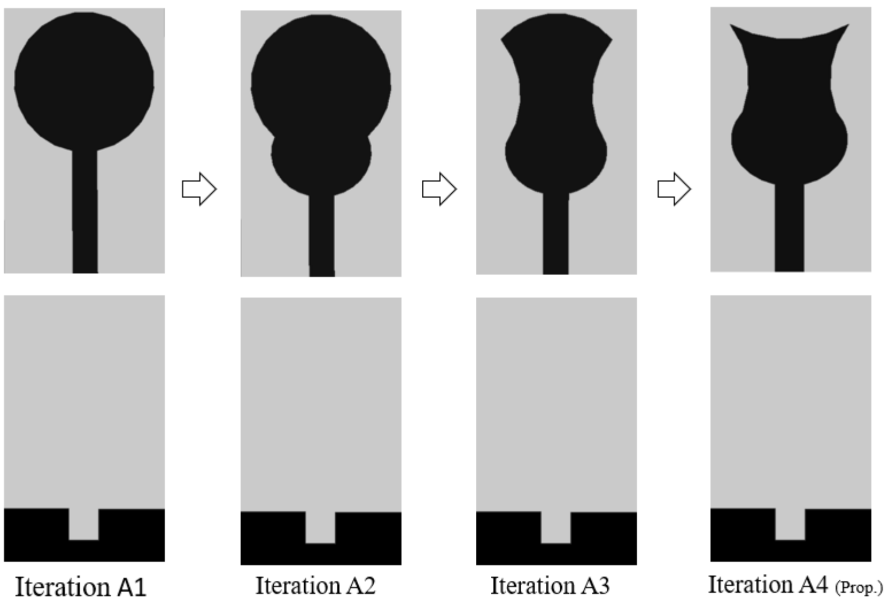

(**a**)

Figure 1. *Cont.*

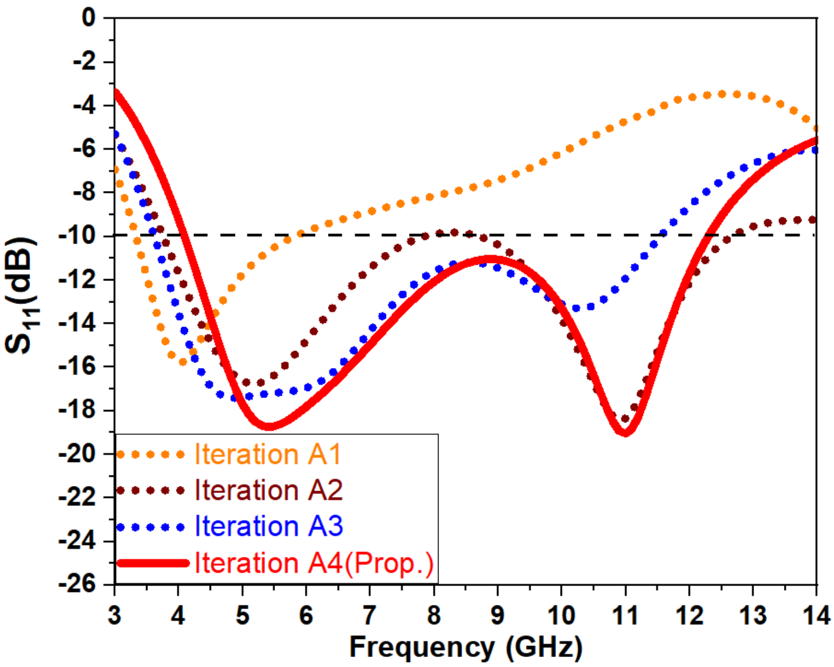

(**b**)

Figure 1. Evolution stages of a radiating element (**a**) radiator structure (**b**) S11 curves.

The proposed single element has an overall size of 20 × 11 × 1.6 mm^3 on the FR4 substrate. The geometrical information and S11 curve are depicted in Figure 2 and Table 1.

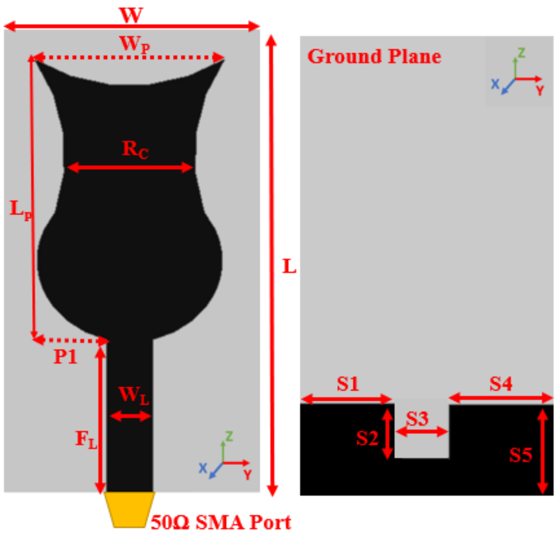

Figure 2. Geometrical information of the antenna.

Table 1. Antenna design parameter values in mm.

W	L	Wp	Lp	P1	Rc	FL	WL	S1	S2	S3	S4	S5
20	11	8.2	11.8	2.8	5.7	6.6	2	4.5	2.3	2	4.5	4

A two-port UWB antenna is built by reproducing the proposed single-element antenna horizontally with a spacing of 0.16 λ. The overall dimension of the proposed two-port antenna is 20 × 29 × 1.6 mm^3 and a redesigned ground plane to decrease mutual coupling. Figure 3 depicts the two-port antenna without DGS and its reflection and transmission coefficients curve. The S-parameters curve shows that the antenna functions from 4 to

12.2 GHz, although field coupling among the antenna's inert ports is significant, especially at lower and higher frequencies. The strong mutual coupling between the ports is even witnessed through the surface current distribution plot of the proposed antenna at the resonating frequency of 6.5 GHz and 10.5 GHz, as depicted in Figure 3c.

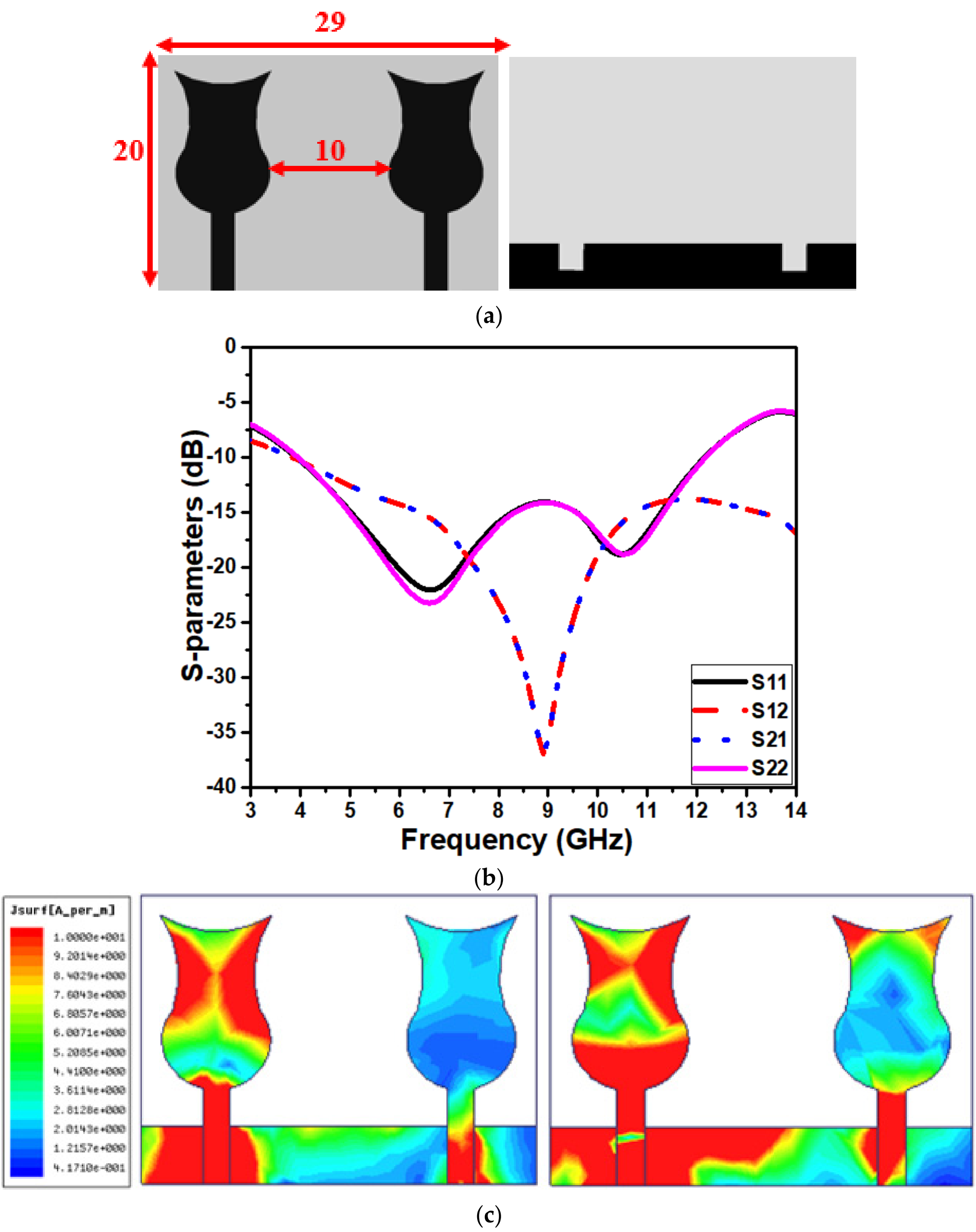

Figure 3. Two-port UWB antenna without decoupling structure: (**a**) antenna (dimensions in mm), (**b**) simulated S-parameters curve, (**c**) surface current distribution at 6.5 GHz (left) and 10.5 GHz (right).

An inverted pendulum-shaped parasitic element is embedded in the ground plane to improve the isolation among the antenna ports. Further, to improve the operating frequency towards the lower side and isolation, an arc is incorporated at the botch edges of the ground plane. The modified antenna configuration operates in the 5–13.5 GHz frequency range with isolation better than 22 dB across the operating frequency. The geometrical information of the proposed antenna and its S-parameters curve is depicted in Figure 4 and Table 2. Ground plane modifications interrupt the uniform current flow and produce additional closed- and open-current channels, preventing mutual coupling. Modifying the ground plane of the proposed antenna lowers mutual coupling by functioning as a band-stop feature.

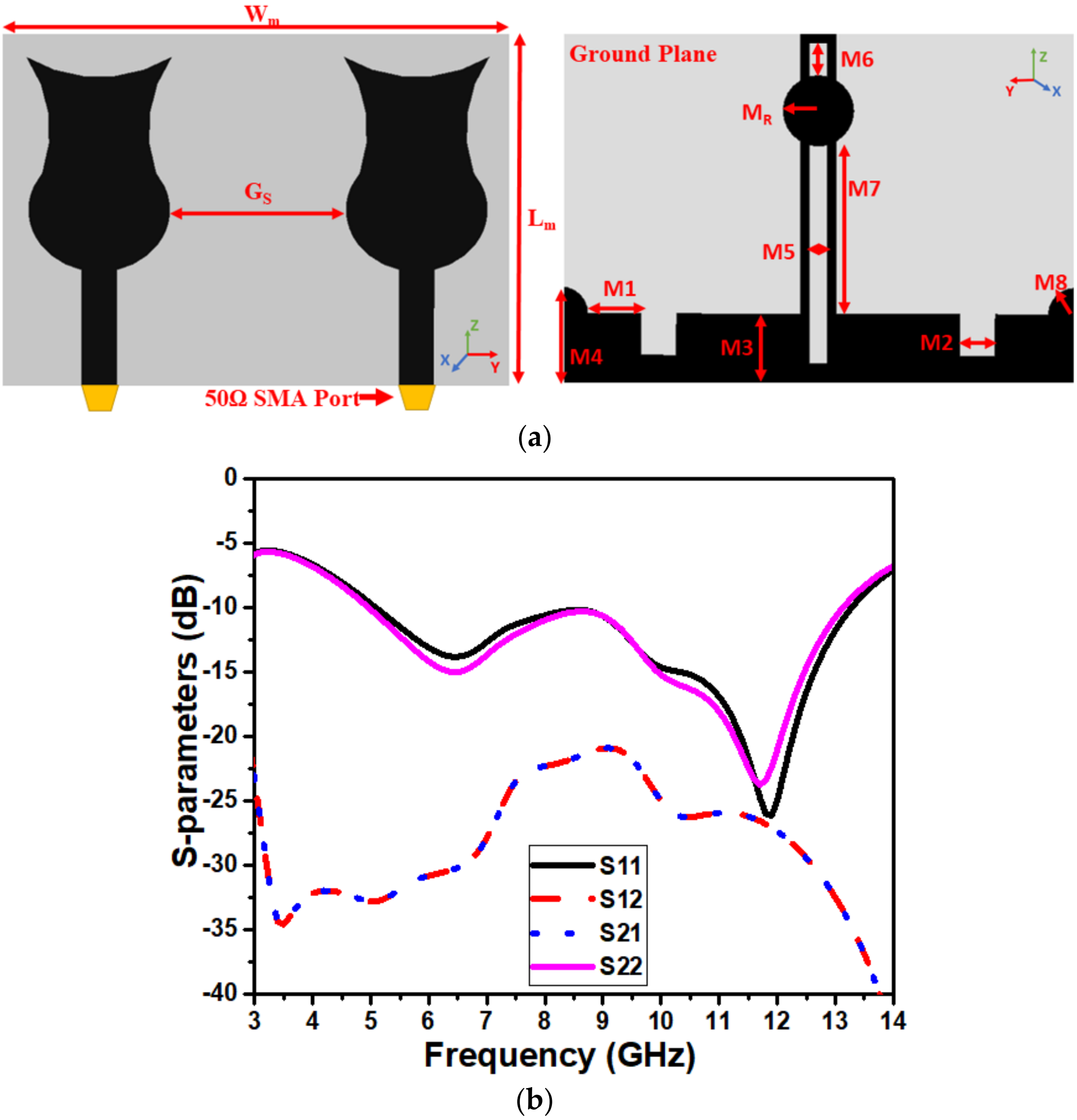

Figure 4. Proposed two-port UWB antenna: (**a**) antenna; (**b**) simulated S-parameters.

Table 2. Geometrical information of the two-port UWB antenna (dimension in mm).

Wm	Lm	Gs	M1	M2	M3	M4	M5	M6	M7	M8	MR
29	20	10	3	2	4	5.5	1	2.2	9.7	1.5	2

3. Parametric Analysis

A comprehensive parametric analysis is used to determine the ideal values of the antenna parameters. In the first stage, the ground plane of the antenna (S5) is lowered in a sequential manner from 10 mm to 8 mm with a step of 2 mm. The antenna's reduced ground plane changes the uniform current distribution and decreases the quality factor, which enhances the impedance bandwidth. The change in the value of the S5 and its impact is illustrated in Figure 5a. The width of the feedline (WL) varies from 1.6 mm to 2.4 mm with a step of 0.2 mm. The value of the WL 1.6 mm provides below −10 dB operating frequency on the lower side; however, at a higher frequency, S11 is above −10 dB, as depicted in Figure 5b. The linear increase in the WL with 0.2 mm improves the impedance bandwidth in a wider frequency range, and the optimal value of the WL is 2 mm. Similarly, the radiator width (Rc) varies from 4.9 mm to 6.3 mm with a step of 0.4 mm. The variation in Rc has a smaller influence on the S11 curve. The value of Rc is selected as 5.7 mm for the optimal operation of the antenna.

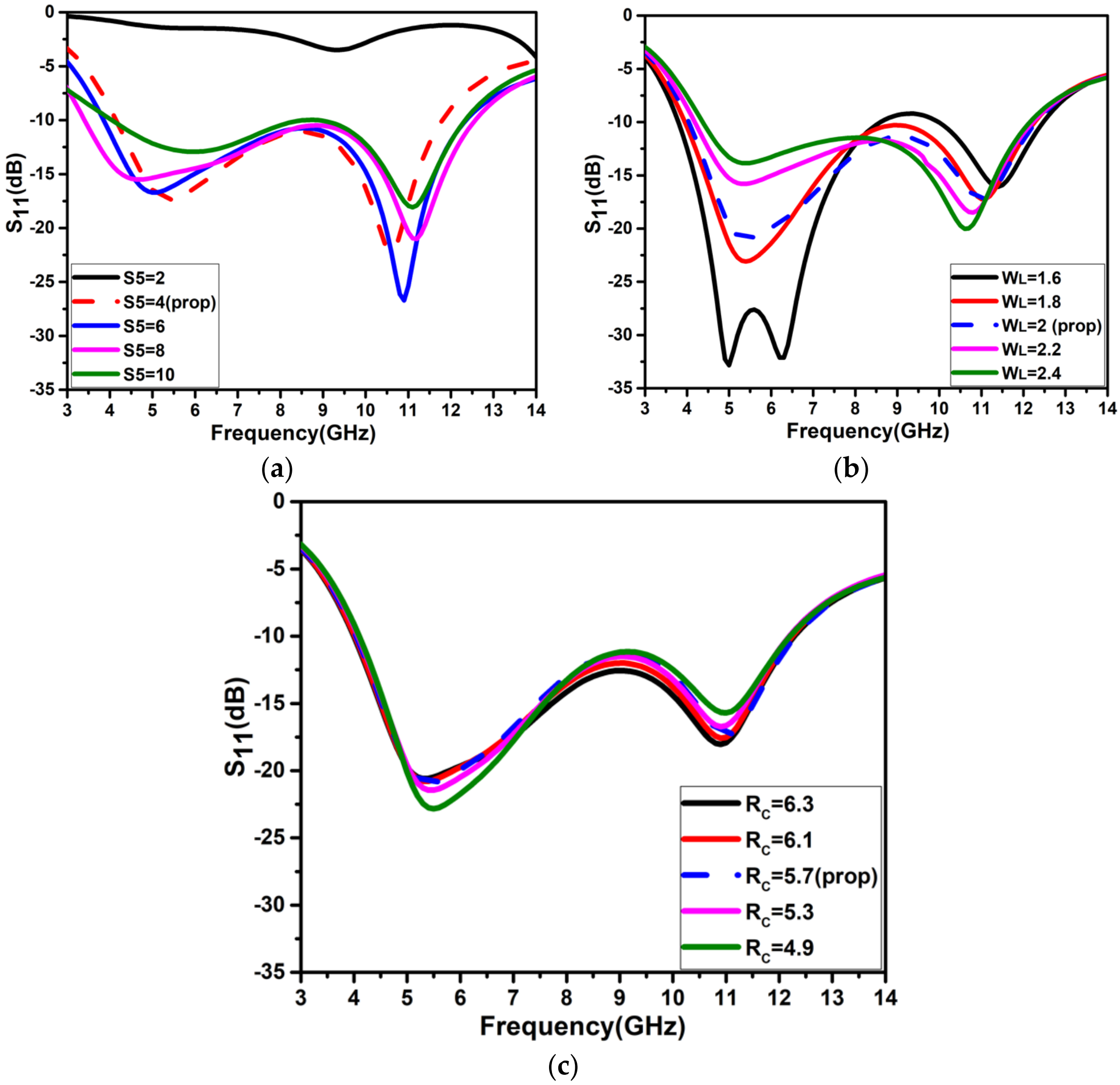

Figure 5. Parametric analysis (dimensions are in mm): (**a**) S5, (**b**) WL, (**c**) Rc.

The UWB antenna is reproduced horizontally with 10 mm edge-to-edge spacing. The distance between the inter elements (GS) is determined by completing a parametric analysis from 9 mm to 10 mm with 1 mm steps. As shown in Figure 6, each incremental value of the GS reflection and transmission coefficients is displayed. The GS value is set to 10 mm. This GS value antenna operates from 5 to 13.5 GHz with isolation of greater than 22 dB over the working frequency range.

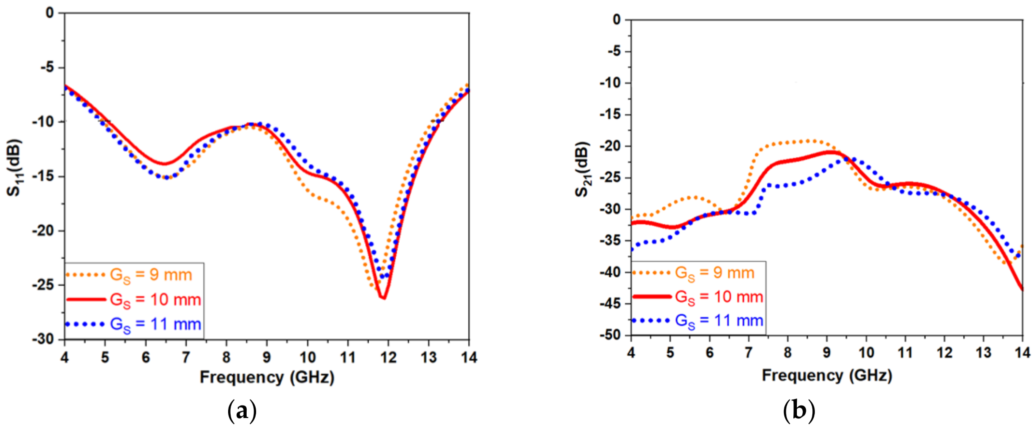

Figure 6. Parametric analysis for edge-to-edge separation in MIMO antenna: (**a**) S11; (**b**) S21.

4. Characteristic Mode Analysis

Characteristic mode analysis (CMA) is a powerful approach for analyzing and designing antennas. CMA is a mathematical approach for determining an antenna's radiation parameters by breaking it into its fundamental modes. The essential concept underlying CMA is to depict the antenna's electromagnetic fields as a linear combination of its characteristic modes. The distinctive modes of an antenna are those that may radiate independently of the other modes. It is feasible to understand the underlying features of the antenna and optimize its performance by dissecting its radiation into its distinctive modes. The CMA approach includes solving an eigenvalue problem to determine the antenna's characteristic modes. The eigenvalues are the frequencies at which the antenna radiates most efficiently, while the eigenvectors describe the radiation pattern's mode shapes and polarization.

In 1965, Robert J. Garbacz was the first to investigate the underlying theory of the CMA that describes the "introduction of modal expansion in electromagnetic scattering on resonance region" [16,17]. A fundamental idea of CMA theory states that the total amount of current that results from an incoming electromagnetic field flowing through an electrically conducting or radiating structure can be expressed as the weighted sum of N transverse eigencurrents (J_i) that are dependent on the excitation vector but also dependent on geometry and material [18,19]. Equation (1) depicts the total current. Modal weight coefficients (β_i) determine eigencurrents' effects on the total current. The entire current creates the radiated electric field since each eigencurrent generates its own.

$$J = \sum_{i=n}^{N} \beta_i \, J_i \tag{1}$$

Each mode's maximum normalized current strength is determined by the modal significance (MS), a crucial parameter of the CMA that also affects that mode's radiation characteristics. Equation (2) may be utilized to determine the MS.

$$MS = \left| \frac{1}{1 + j\lambda_i} \right| \tag{2}$$

In Equation (2), MS is inversely proportional to the eigenvalue (λ_i). The λ_i can be computed using a method of moment matrix ($[Z]$) and an eigencurrent, as described in Equations (3) and (4).

$$[Z] = [R] + j[X] \tag{3}$$

$$[X]\, J_i = \lambda_i \, [R] \, J_i \tag{4}$$

The real and imaginary components of the Z are defined by R and X. The importance of the eigenvalues lies in the ability to forecast conducting structure resonance or internal energy using these values, as listed in Table 3. The characteristic angle (CA) can be used to explain the phase difference in the antenna's electric field and surface current. Equation (5) helps to compute the CA (α_(*i*)).

$$\alpha_i = 180^0 - tan^{-1}\lambda_i \quad (5)$$

Table 3. Significance of eigenvalues.

Eigenvalues (λ_i)	CA (α_i)	Significance
$\lambda_i < 0$	$180 < \alpha_i < 270$	Electric energy
$\lambda_i = 0$	$\alpha_i = 180$	Resonating point
$\lambda_i > 0$	$90 < \alpha_i < 180$	Magnetic energy

In order to determine the significant modes and their contribution to antenna radiation, the proposed two-port antenna is analyzed for the CMA. The MS and CA of the five modes of the proposed antenna are illustrated in Figure 7. The modes of the antenna are considered significant if the value of the MS is greater than 0.707 [20]. At the resonant frequency of 6.4 GHz except mode 3, all other modes are significant and have MS greater than 0.707 and a CA of approximately 180 degrees. These values depict that modes 1, 2, 4, and 5 are resonant modes. Similarly, at the resonant frequency of 11.9 GHz, all five modes are significant and resonating modes, except for mode 5, and CA at 11.9 GHz in Figure 7d describes how mode 5 stores energy in the form of magnetic energy as its CA values fall below 180 degrees.

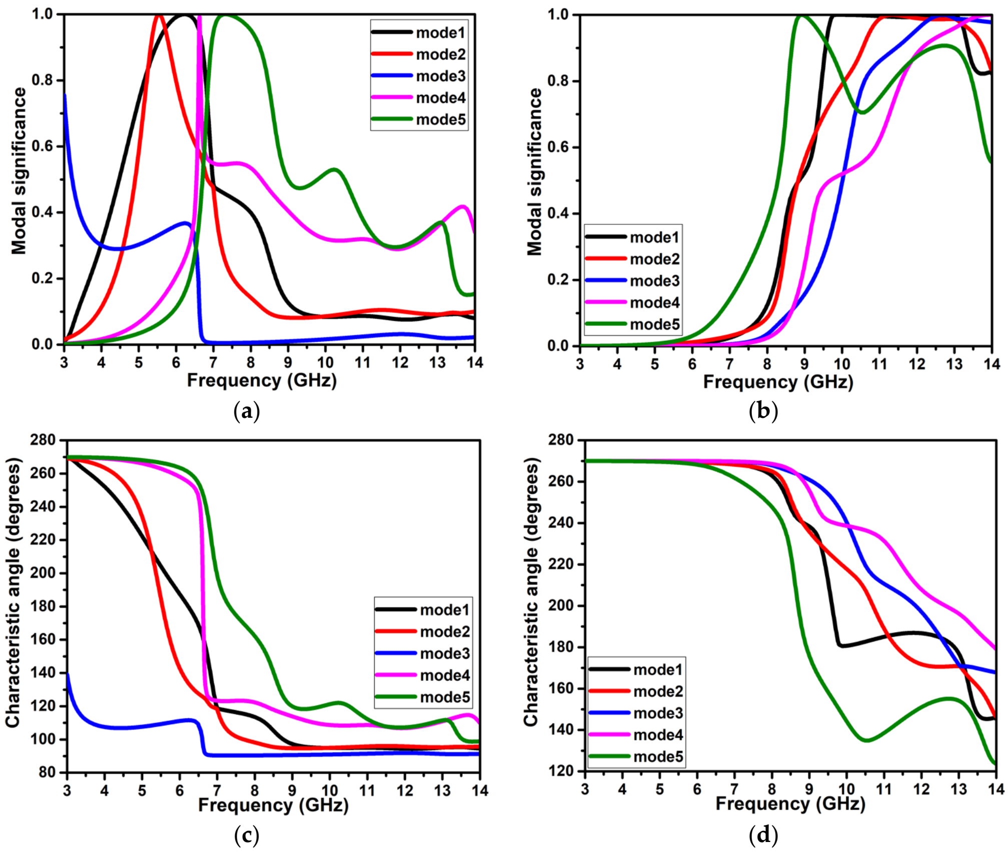

Figure 7. The proposed antenna CMA analysis: MS at (**a**) 6.4 GHz and (**b**) 11.9 GHz and CA at (**c**) 6.4 GHz and (**d**) 11.9 GHz.

The surface current distribution and far-field pattern of the various individual modes at the resonant frequencies of 6.4 GHz and 11.9 GHz are depicted in Figure 8. The individual modes contribute to the antenna radiation, except for mode 3 at 6.4 GHz and mode 5 at 11.9 GHz. These modes help the antenna to radiate in quasi-bidirectional and omnidirectional correspondingly in E and H planes.

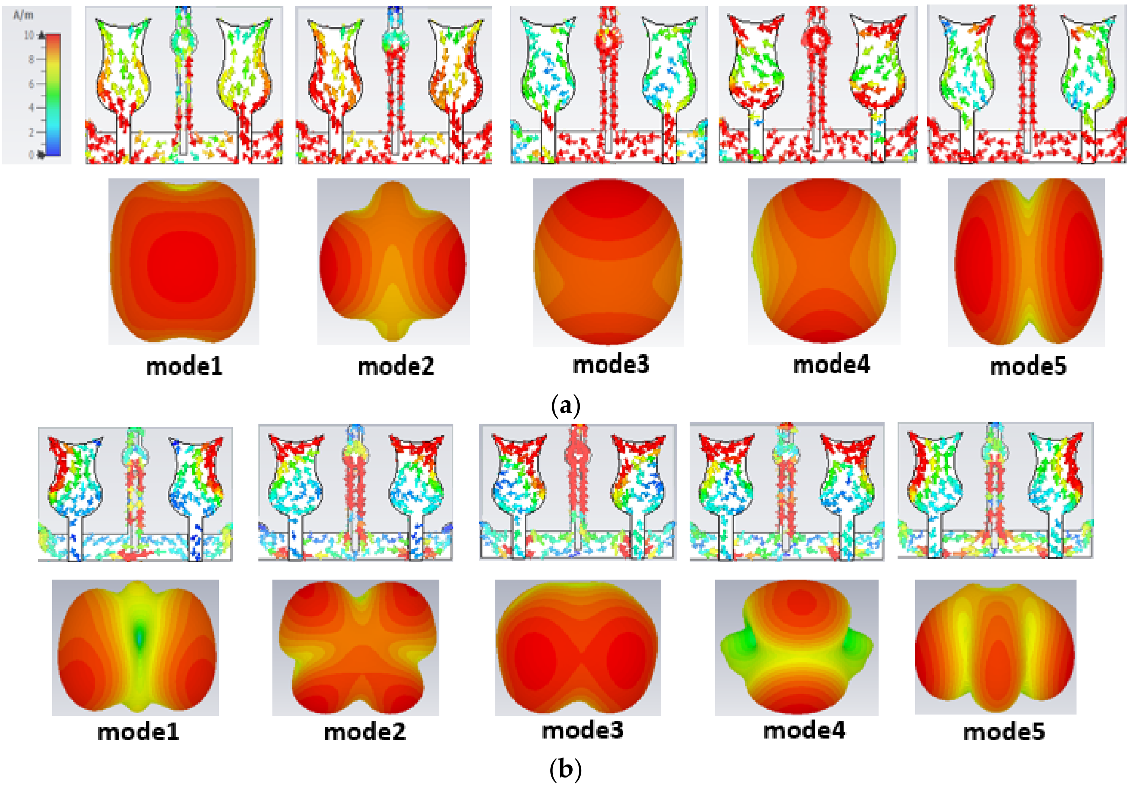

Figure 8. Current distribution and far-field pattern at various modes at (**a**) 6.4 GHz and (**b**) 11.9 GHz.

5. Results and Discussion

The designed two-port UWB antenna is fabricated on an FR-4 substrate with a thickness of 1.6 mm, dielectric constant of 4.4, and loss tangent of 0.02. The developed two-port UWB antenna is examined for scattering parameters, radiation properties, MIMO diversity features, and time domain characteristics using a high-frequency structure simulator (HFSS). The prototype's results tend to be consistent with the simulated outcomes. Due to manufacturing and testing tolerances, a minor variance is noted.

5.1. Scattering Parameters

The developed two-port UWB antenna is measured using an Agilent N5247A vector network analyzer. The impedance bandwidth of the proposed antenna is from 5 to 13.5 GHz. The DGS, as a decoupling structure, is used for enhancing isolation among the inter ports of the proposed antenna. Across the antenna's operating frequency, isolation is better than 21 dB in both simulated and measured scenarios. The S-parameters of the proposed antenna are illustrated in Figure 9.

5.2. Current Distribution

The surface current distribution of the proposed antenna is performed at resonant frequencies of 6.4 GHz and 11.9 GHz by stimulating one port and terminating the other port of the antenna. The current plot of these frequencies shows maximum current concentration across the excited element, ground plane, and negligible field influence on the neighboring element, as depicted in Figure 10. It assures the effectiveness of the decoupling structure developed to decrease mutual coupling among the MIMO antenna elements.

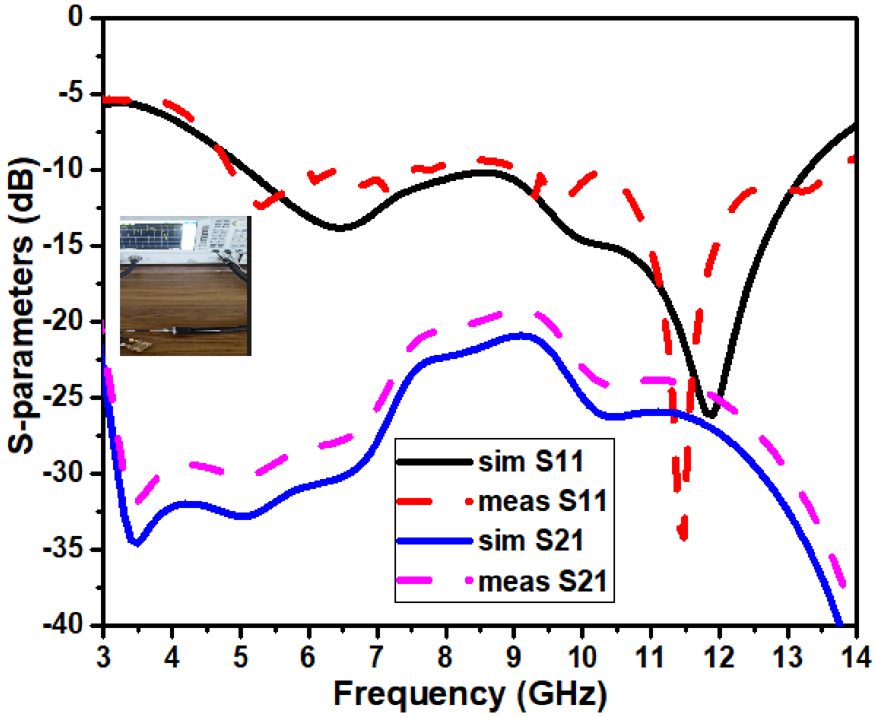

Figure 9. S-parameters of the proposed antenna.

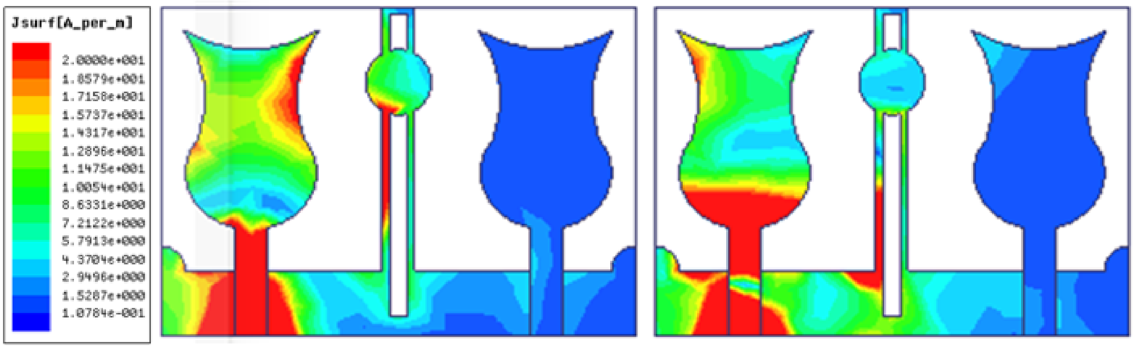

(**a**) (**b**)

Figure 10. Surface current distribution plot: (**a**) 6.4 GHz and (**b**) 11.9 GHz.

5.3. Radiation Properties

At the resonant frequencies, 6.4 GHz and 11.9 GHz, a two-dimensional radiation pattern of the proposed antenna is plotted in XZ and YZ planes, as represented in Figure 11. The co and cross radiation pattern at the E and H planes is measured by exciting one port and terminating the other with the matched load at 50 Ω. The simulated and measured radiation pattern at the two principal planes, E and H, correspondingly demonstrates the quasi-bidirectional and omnidirectional. The simulated and measured gain of the antenna against the frequency is depicted in Figure 11d. The maximum and minimum gain of the antenna is 5.5 dBi, and 0.4 dBi is observed at frequencies of 9.5 GHz and 4.5 GHz.

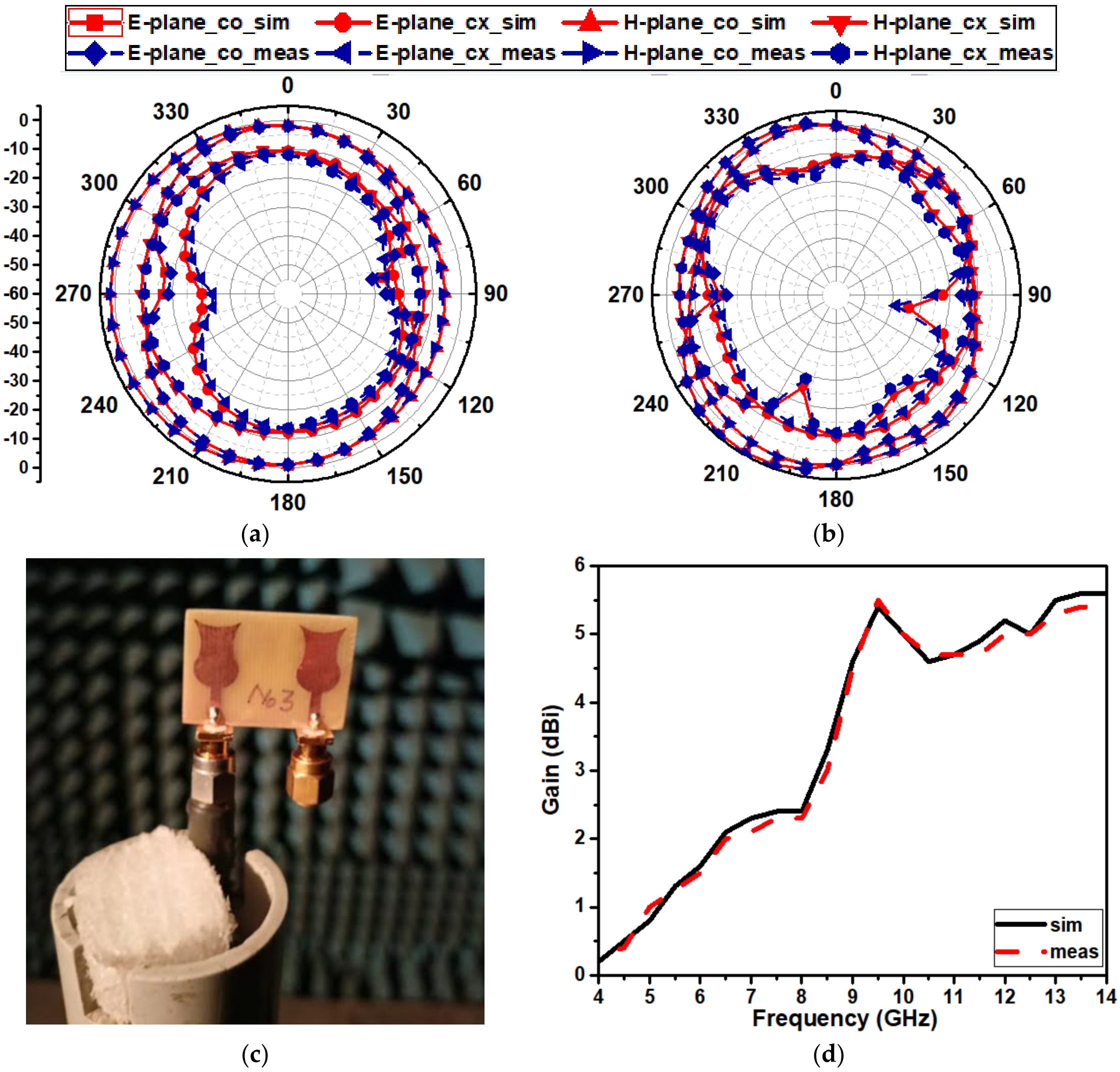

Figure 11. Radiation plot at: (**a**) 6.4 GHz, (**b**) 11.9 GHz, (**c**) antenna measurement, and (**d**) gain vs. frequency curve.

5.4. Diversity Features

The MIMO diversity features of the proposed antenna are evaluated. In MIMO systems, the envelope correlation coefficient (ECC) defines the level of coupling between the antenna elements. The signal-to-interference ratio is described by diversity gain (DG), which is connected with the ECC. The threshold values for ECC and DG are less than 0.5 and approximately 10 dB. The mean effective gain (MEG) refers to the average gain experienced by the transmitted signals in an MIMO channel. It is a measure of the combined influence of antenna gain, propagation environment, and channel spatial features. The total active reflection coefficient (TARC) of an N-port antenna is the square root of the total of all outgoing powers at the ports divided by the sum of all incident powers at the ports. An MIMO antenna system's channel capacity loss (CCL) refers to the system's highest attainable data rate or capacity in a specific communication channel. The presence of noise, interference, and the features of the MIMO antenna system all impact the channel capacity. MEG, TARC, and CCL acceptable values are <-3 dB, <-10 dB, and <0.4 bps/Hz. The proposed antenna demonstrates the value of diversity features as ECC $<$ 0.002, DG is approximately 10 dB, MEG < −3 dB, TARC < −10 dB, and CCL < 0.3 bps/Hz, as depicted in Figure 12, and are computed using Equations (6)–(10).

$$ECC = \frac{\left|S_{11}^{*}\, S_{12} + S_{21}^{*}\, S_{22}\right|^2}{\left(1 - |S_{11}|^2 - |S_{21}|^2\right)\left(1 - |S_{22}|^2 - |S_{12}|^2\right)} \tag{6}$$

$$DG = 10\sqrt{1 - ECC} \tag{7}$$

$$TARC = \sqrt{\frac{(S_{11} + S_{12})^2 + (S_{21} + S_{22})^2}{2}} \tag{8}$$

$$CCL = -log_2 \det(\alpha)^R \tag{9}$$

where α^R is the receiving antenna correlation matrix for two elements α^R as follows:

$$\alpha^R = \begin{vmatrix} \rho_{11} & \rho_{12} \\ \rho_{21} & \rho_{22} \end{vmatrix}$$

where $\rho_{ii} = 1 - \left|\sum_{n=1}^{N=2} S_{i,n}^{*}\, S_{n,i}\right|$ and $\rho_{ij} = -\left|\sum_{n=1}^{N=2} S_{i,n}^{*}\, S_{n,j}\right|$ for $i, j = 1,\ 2$.

$$MEG_i = 0.5\left(1 - \sum_{j=1}^{M} |S_{ij}|\right) \tag{10}$$

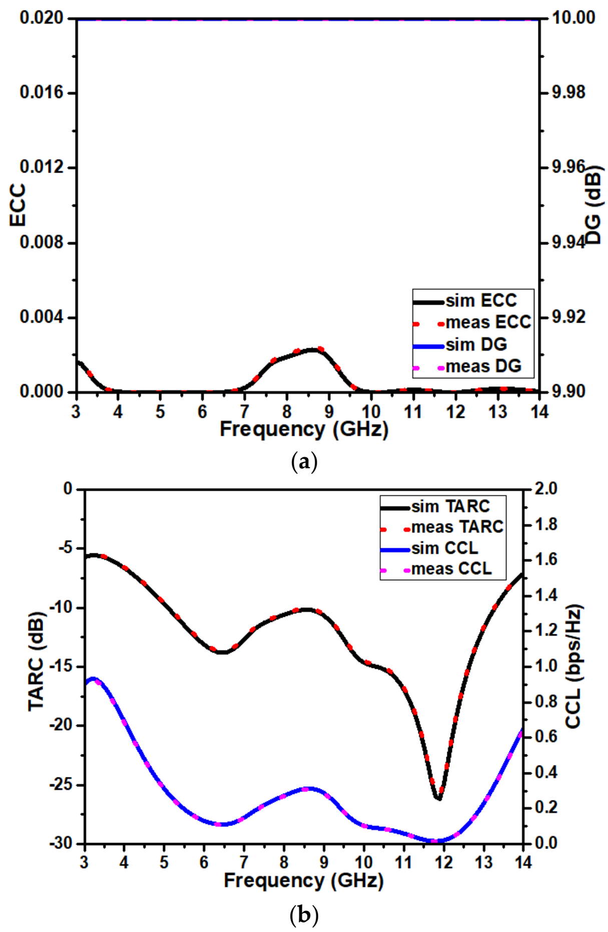

Figure 12. *Cont.*

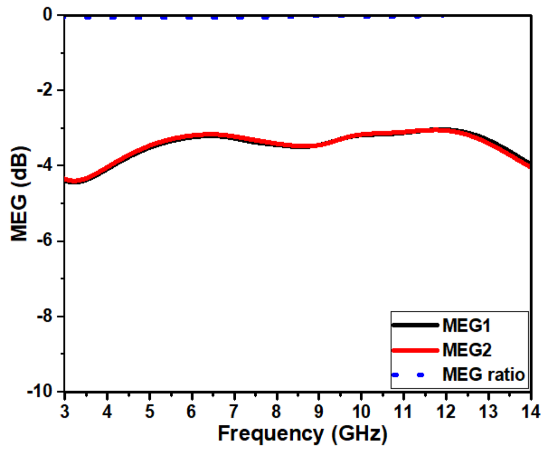

(c)

Figure 12. MIMO diversity features: (**a**) ECC and DG, (**b**) TARC and CCL, and (**c**) MEG.

5.5. Time Domain Features

The proposed two-port UWB antenna is configured in face-to-face and side-to-side arrangement with a separation of 100 mm to perform time domain features, such as transfer function, phase response, group delay (GD), and fidelity factor (FF). The transfer function describes the amount of correlation among the antenna elements in MIMO. The phase response illustrates the phase linearity in the transceiver system. The transfer function and phase response of the proposed antenna are illustrated in Figure 13a,b. The figure shows that the transfer function is better than −25 dB, and the phase is linear across the antenna's operating frequency. The GD of the antenna depicts the phase variation in concordance with the angular frequency, as shown in Equation (11). The FF describes the synchronization of the shape of the output and input signal, not the signal's amplitude. The FF helps to realize the faithful reproduction of the signal at the receiver and is computed using Equations (12)–(14). The GD and FF of the proposed antenna are less than 1 ns and better than 0.9, respectively, as shown in Figure 13c,d.

$$GD = -\frac{d\varphi(\omega)}{d\omega} \tag{11}$$

The normalized transmitted and received pulse is described to evaluate FF.

$$T_s^n = \frac{T_s(t)}{\sqrt{\int_{-\infty}^{\infty} |T_s(t)|^2 dt}} \tag{12}$$

$$R_s^n = \frac{R_s(t)}{\sqrt{\int_{-\infty}^{\infty} |R_s(t)|^2 dt}} \tag{13}$$

$$FF = \max \int\limits_{-\infty}^{\infty} T_s^n(t) \;\; R_s^n(t+\tau) dt \tag{14}$$

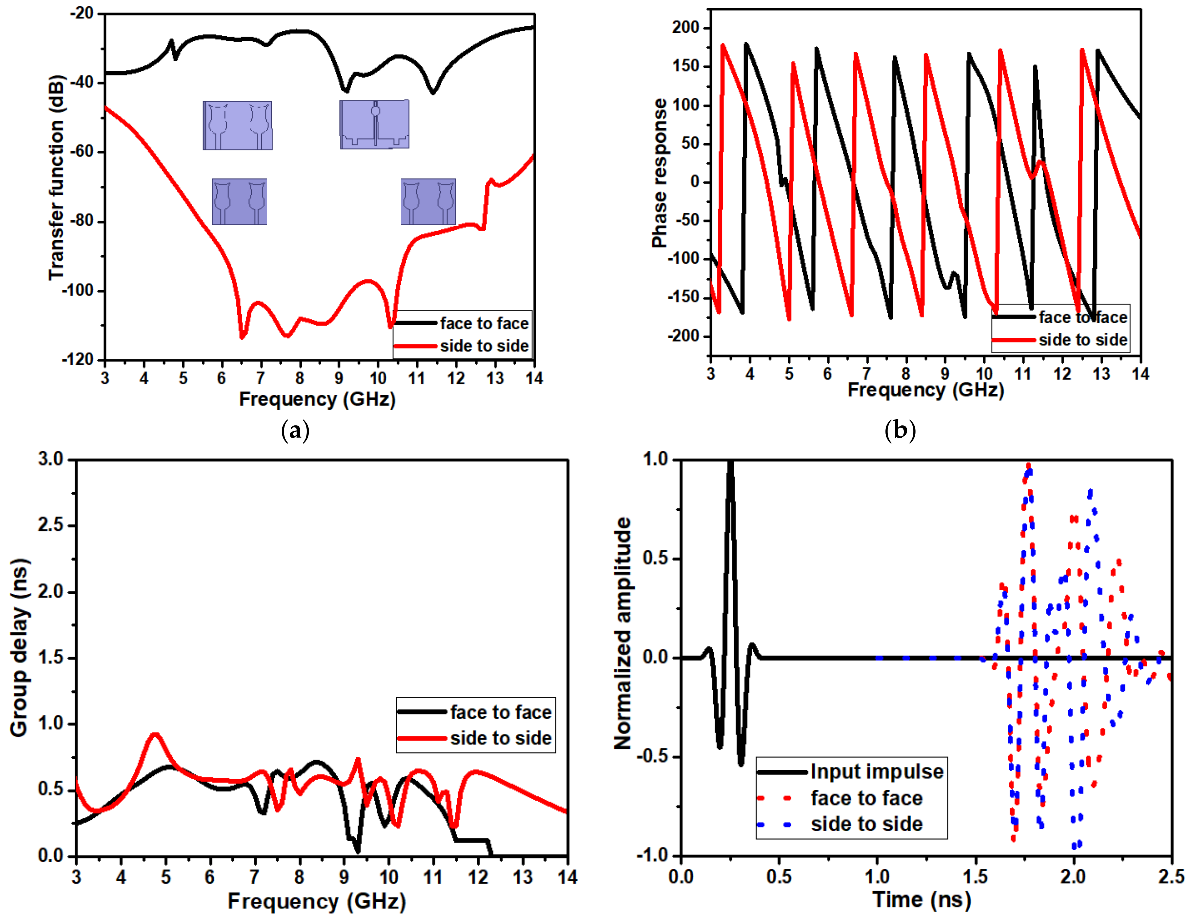

Figure 13. Time domain features of the proposed antenna: (**a**) transfer function, (**b**) phase response, (**c**) group delay, and (**d**) normalized amplitude.

6. Comparative Analysis

To highlight the advantages of the proposed MIMO antenna, Table 4 compiles the results of several antennas from the literature. In comparison to past studies, the proposed antenna has a larger bandwidth, relatively good isolation, and diversity features, as shown in Table 4.

Table 4. Comparative analysis of the proposed antenna.

Ref	Techniques Used	Dimension (mm^3)	Impedance BANDWIDTH (BW) (GHz)/Fractional BW %	Peak Gain (dBi)	Isolation (dB)	ECC	DG	MEG	TARC	CCL
[21]	Orthogonal	35 × 35 × 1	3–12/120	4.6	>20	<0.3	-	<−3	-	-
[22]	Parasitic elements	30 × 40 × 0.8	3.1–10.6/109	-	>15	<0.15	-	-	-	-
[23]	DGS	50 × 30 × 1.6	2.5–14.5/141	4.3	>20	<0.04	>7.4	-	-	-
[24]	DGS	36 × 18 × 1.6	3.2–12/115	4	>22	<0.01	-	-	-	<0.4
[25]	DGS	30 × 30 × 1.6	2.6–12/128	5.5	>20	<0.01	-	-	-	-
[26]	Coplanar waveguide	50 × 60 × 1.6	2.98–10/108	2.5	>31.4	<0.5	≈ 10	-	-	-
[27]	DGS	35 × 50 × 1.6	3–11/114	5.5	>25	<0.004	-	-	-	-
[28]	DGS	35 × 46 × 1.6	2.1–11.4/137	1.5	>15	<0.04	≈ 10	-	-	-
proposed	DGS	20 × 29 × 1.6	5–13.5/92	5.5	>21	<0.002	≈ 10	<−3	<−10	<0.3

Note: “-”—NA.

7. Conclusions

This research presents a compact vase-shaped UWB MIMO antenna. The unique DGS as a decoupling structure improves the isolation between the inter elements. The inverted pendulum-shaped decoupling structure offers greater than 21 dB isolation over the antenna's 5–13.5 GHz operating frequency range. The designed UWB MIMO antenna's performance characteristics, such as scattering parameters, radiation properties, CMA, diversity features, and time domain characteristics, are examined. The simulated and measured results are consistent. The antenna results show that the developed antenna is appropriate for wireless applications.

Author Contributions: Conceptualization, S.B.K., P.K. (Praveen Kumar), T.A., P.K. (Pradeep Kumar), S.P. and R.C.B.; methodology, S.B.K., P.K. (Praveen Kumar), T.A., P.K. (Pradeep Kumar), S.P. and R.C.B.; software, S.B.K., P.K. (Praveen Kumar), and T.A.; formal analysis, S.B.K., P.K. (Praveen Kumar), T.A., P.K. (Pradeep Kumar), S.P. and R.C.B.; investigation, S.B.K., P.K. (Praveen Kumar), T.A., P.K. (Pradeep Kumar), S.P. and R.C.B.; resources, S.B.K., P.K. (Praveen Kumar), T.A., P.K. (Pradeep Kumar), S.P. and R.C.B.; data curation, S.B.K., P.K. (Praveen Kumar), T.A. and R.C.B.; writing—original draft preparation S.B.K., P.K. (Praveen Kumar), T.A., P.K. (Pradeep Kumar), S.P. and R.C.B.; writing—review and editing, S.B.K., P.K. (Praveen Kumar), T.A, P.K. (Pradeep Kumar), S.P. and R.C.B.; visualization, S.B.K., P.K. (Praveen Kumar), T.A., P.K. (Pradeep Kumar), S.P. and R.C.B.; supervision, T.A, P.K. (Pradeep Kumar), and R.C.B. All authors have read and agreed to the published version of the manuscript.

Funding: This research received no external funding.

Data Availability Statement: The data are contained within the article.

Conflicts of Interest: The authors declare no conflict of interest.

References

1. Galvan-Tejada, G.M.; Peyrot-Solis, M.A.; Aguilar, H.J. *Ultra Wideband Antennas: Design, Methodologies, and Performance*; CRC Press: Boca Raton, FL, USA, 2017.
2. Chen, Z.N.; Chia, M.Y.W. *Broadband Planar Antennas: Design and Applications*; John Wiley & Sons: Hoboken, NJ, USA, 2006.
3. Devana, V.K.R.; Satyanarayana, V.; Lakshmi, A.V.; Sukanya, Y.; Kumar, C.M.; Ponnapalli, V.P.; Jagadeesh Babu, K. A novel compact fractal UWB antenna with dual band notched characteristics. *Analog. Integr. Circuits Signal Process.* **2022**, *110*, 349–360. [CrossRef]
4. Pandhare, R.A.; Abegaonkar, M.P.; Dhote, C. UWB antenna with novel FSS reflector for the enhancement of the gain and bandwidth. *Int. J. Microw. Wirel. Technol.* **2022**, *14*, 1353–1368. [CrossRef]
5. Zaidi, A.; Awan, W.A.; Ghaffar, A.; Alzaidi, M.S.; Alsharef, M.; Elkamchouchi, D.H.; Ghoneim, S.S.; Alharbi, T.E. A low profile ultra-wideband antenna with reconfigurable notch band characteristics for smart electronic systems. *Micromachines* **2022**, *13*, 1803. [CrossRef] [PubMed]
6. Uwiringiyimana, J.P.; Khayam, U.; Montanari, G.C. Design and implementation of ultra-wide band antenna for partial discharge detection in high voltage power equipment. *IEEE Access* **2022**, *10*, 10983–10994. [CrossRef]
7. Saeidi, T.; Alhawari, A.R.; Almawgani, A.H.; Alsuwian, T.; Imran, M.A.; Abbasi, Q. High gain compact UWB antenna for ground penetrating radar detection and soil inspection. *Sensors* **2022**, *22*, 5183. [CrossRef]
8. Abbas, A.; Hussain, N.; Sufian, M.A.; Jung, J.; Park, S.M.; Kim, N. Isolation and gain improvement of a rectangular notch UWB-MIMO antenna. *Sensors* **2022**, *22*, 1460. [CrossRef]
9. Balaji, V.R.; Addepalli, T.; Desai, A.; Nella, A.; Nguyen, T.K. An inverted L-strip loaded ground with hollow semi-hexagonal four-element polarization diversity UWB-MIMO antenna. *Trans. Emerg. Telecommun. Technol.* **2022**, *33*, e4381. [CrossRef]
10. Ahmed, B.T.; Rodríguez, I.F. Compact high isolation UWB MIMO antennas. *Wirel. Netw.* **2022**, *28*, 1977–1999. [CrossRef]
11. Mu, W.; Lin, H.; Wang, Z.; Li, C.; Yang, M.; Nie, W.; Wu, J. A flower-shaped miniaturized UWB-MIMO antenna with high isolation. *Electronics* **2022**, *11*, 2190. [CrossRef]
12. Sharawi, M.S. Current misuses and future prospects for printed multiple-input, multiple-output antenna systems [wireless corner]. *IEEE Antennas Propag. Mag.* **2017**, *59*, 162–170. [CrossRef]
13. Kumar, P.; Pathan, S.; Vincent, S.; Kumar, O.P.; Yashwanth, N.; Kumar, P.; Shetty, P.R.; Ali, T. A Compact Quad-Port UWB MIMO Antenna with Improved Isolation Using a Novel Mesh-Like Decoupling Structure and Unique DGS. *IEEE Trans. Circuits Syst. II Express Briefs* **2023**, *70*, 949–953. [CrossRef]
14. Kumar, P.; Ali, T.; Pai, M.M. A compact highly isolated two-and four-port ultrawideband Multiple Input and Multiple Output antenna with Wireless LAN and X-band notch characteristics based on Defected Ground Structure. *Int. J. Commun. Syst.* **2022**, *35*, e5331. [CrossRef]

15. Kumar, P.; Pathan, S.; Kumar, O.P.; Vincent, S.; Nanjappa, Y.; Kumar, P.; Shetty, P.; Ali, T. Design of a Six-Port Compact UWB MIMO Antenna With a Distinctive DGS for Improved Isolation. *IEEE Access* **2022**, *10*, 112964–112974. [CrossRef]
16. Garbacz, R.J. Modal expansions for resonance scattering phenomena. *Proc. IEEE* **1965**, *53*, 856–864. [CrossRef]
17. Garbacz, R.; Turpin, R. A generalized expansion for radiated and scattered fields. *IEEE Trans. Antennas Propag.* **1971**, *19*, 348–358. [CrossRef]
18. Austin, B.A.; Murray, K.P. The application of characteristic-mode techniques to vehicle-mounted NVIS antennas. *IEEE Antennas Propag. Mag.* **1998**, *40*, 7–21. [CrossRef]
19. Kim, J.; Qu, L.; Jo, H.; Zhang, R.; Kim, H. A MIMO antenna design based on the characteristic mode. *Microw. Opt. Technol. Lett.* **2017**, *59*, 893–898. [CrossRef]
20. Adams, J.J.; Genovesi, S.; Yang, B.; Antonino-Daviu, E. Antenna Element Design Using Characteristic Mode Analysis: Insights and research directions. *IEEE Antennas Propag. Mag.* **2022**, *64*, 32–40. [CrossRef]
21. Zhu, J.; Li, S.; Feng, B.; Deng, L.; Yin, S. Compact dual-polarized UWB quasi-self-complementary MIMO/diversity antenna with band-rejection capability. *IEEE Antennas Wirel. Propag. Lett.* **2015**, *15*, 905–908. [CrossRef]
22. Deng, J.Y.; Guo, L.X.; Liu, X.L. An ultrawideband MIMO antenna with a high isolation. *IEEE Antennas Wirel. Propag. Lett.* **2015**, *15*, 182–185. [CrossRef]
23. Iqbal, A.; Saraereh, O.A.; Ahmad, A.W.; Bashir, S. Mutual coupling reduction using F-shaped stubs in UWB-MIMO antenna. *IEEE Access* **2017**, *6*, 2755–2759. [CrossRef]
24. Srivastava, G.; Mohan, A. Compact MIMO slot antenna for UWB applications. *IEEE Antennas Wirel. Propag. Lett.* **2015**, *15*, 1057–1060. [CrossRef]
25. Jabire, A.H.; Ghaffar, A.; Li, X.J.; Abdu, A.; Saminu, S.; Alibakhshikenari, M.; Falcone, F.; Limiti, E. Metamaterial based design of compact UWB/MIMO monopoles antenna with characteristic mode analysis. *Appl. Sci.* **2021**, *11*, 1542. [CrossRef]
26. Nie, L.Y.; Lin, X.Q.; Xiang, S.; Wang, B.; Xiao, L.; Ye, J.Y. High-isolation two-port UWB antenna based on shared structure. *IEEE Trans. Antennas Propag.* **2020**, *68*, 8186–8191. [CrossRef]
27. Wang, L.; Du, Z.; Yang, H.; Ma, R.; Zhao, Y.; Cui, X.; Xi, X. Compact UWB MIMO antenna with high isolation using fence-type decoupling structure. *IEEE Antennas Wirel. Propag. Lett.* **2019**, *18*, 1641–1645. [CrossRef]
28. Agarwal, M.; Dhanoa, J.K.; Khandelwal, M.K. Two-port hexagon shaped MIMO microstrip antenna for UWB applications integrated with double stop bands for WiMax and WLAN. *AEU-Int. J. Electron. Commun.* **2021**, *138*, 153885. [CrossRef]